Structure of a Complete Integrin Ectodomain in a Physiologic Resting State and Activation and Deactivation by Applied Forces

Jianghai Zhu,[1,2] Bing-Hao Luo,[1,2,3] Tsan Xiao,[1,2,4] Chengzhong Zhang,[1] Noritaka Nishida,[1,5] and Timothy A. Springer[1,*]

[1]The Immune Disease Institute and Department of Pathology, Harvard Medical School, 200 Longwood Avenue, Boston, MA 02115, USA
[2]These authors contributed equally to this work
[3]Present address: Department of Biological Sciences, 202 Life Sciences Building, Louisiana State University, Baton Rouge, LA 70803, USA
[4]Present address: Laboratory of Immunology, Structural Immunobiology Section, National Institute of Allergy and Infectious Diseases, National Institutes of Health, 4 Center Drive, Bethesda, MD 20892, USA
[5]Present address: Graduate School of Pharmaceutical Sciences, The University of Tokyo, Hongo, Bunkyo-ku, Tokyo 113-0033, Japan
*Correspondence: springer@idi.harvard.edu
DOI 10.1016/j.molcel.2008.11.018

SUMMARY

The complete ectodomain of integrin $\alpha_{IIb}\beta_3$ reveals a bent, closed, low-affinity conformation, the β knee, and a mechanism for linking cytoskeleton attachment to high affinity for ligand. Ca and Mg ions in the recognition site, including the synergistic metal ion binding site (SyMBS), are loaded prior to ligand binding. Electrophilicity of the ligand-binding Mg ion is increased in the open conformation. The β_3 knee passes between the β_3-PSI and α_{IIb}-knob to bury the lower β leg in a cleft, from which it is released for extension. Different integrin molecules in crystals and EM reveal breathing that appears on pathway to extension. Tensile force applied to the extended ligand-receptor complex stabilizes the closed, low-affinity conformation. By contrast, an additional lateral force applied to the β subunit to mimic attachment to moving actin filaments stabilizes the open, high-affinity conformation. This mechanism propagates allostery over long distances and couples cytoskeleton attachment of integrins to their high-affinity state.

INTRODUCTION

Integrins are cell adhesion receptors that transmit bidirectional signals across the plasma membrane and link the extracellular environment to the actin cytoskeleton. The conformation of the integrin extracellular domain and its affinity for ligand are dynamically regulated by a process termed inside-out signaling. By coupling to the actin cytoskeleton, integrins promote firm adhesion and provide traction for lamellipodium protrusion and locomotion. In migrating cells, the adhesiveness of integrins is spatially and temporally regulated so that integrins are activated near the leading edge to support lamellipod extension and deactivated near the trailing edge to facilitate uropod retraction and internalization (Alon and Dustin, 2007; Arnaout et al., 2005;

Broussard et al., 2008; Evans and Calderwood, 2007; Luo et al., 2007).

Integrin $\alpha_{IIb}\beta_3$, the most abundant receptor on platelets, binds to fibrinogen and von Willebrand factor and mediates platelet aggregation and association with injured vessel walls. Inherited mutations in the α_{IIb} or β_3 subunits result in the bleeding disorder Glanzmann's thrombasthenia. Antagonists to $\alpha_{IIb}\beta_3$ are prescribed for the prevention of thrombosis (see Springer et al., 2008; Xiao et al., 2004, and references therein).

The integrin α and β subunits have large N-terminal extracellular domains, single-pass transmembrane domains, and usually short C-terminal cytoplasmic domains. The entire ectodomain of $\alpha_V\beta_3$ crystallized in a bent conformation revealed 10 of 12 domains (Xiong et al., 2001, 2002, 2004). A ligand-binding head formed by both subunits is followed in each subunit by legs that connect to transmembrane domains. The knees between the upper and lower legs are extremely bent. Integrin epidermal growth factor-like (I-EGF) domains 1 and 2 at the β knee were disordered in the previous $\alpha_V\beta_3$ structure. Crystals of β_2 leg fragments containing I-EGF domains 1 and 2 have been solved in two different orientations (Shi et al., 2007), but the conformation of these domains in the bent integrin conformation remains unknown.

Subsequent to the $\alpha_V\beta_3$ crystal structure, mutational studies on cell-surface integrins and EM studies on $\alpha_V\beta_3$, $\alpha_L\beta_2$, and $\alpha_X\beta_2$ integrins demonstrated that the bent conformation is the physiologically relevant, low-affinity integrin conformation (Nishida et al., 2006; Takagi et al., 2002). Nonetheless, a cryo-EM study on $\alpha_{IIb}\beta_3$ revealed a different, less-compact conformation with a different arrangement of leg domains (Adair and Yeager, 2002). Furthermore, two recent studies have revealed extended conformations of $\alpha_{IIb}\beta_3$ but failed to find a bent conformation (Rocco et al., 2008; Ye et al., 2008). Crystal structure studies on $\alpha_{IIb}\beta_3$ are important to resolve these controversies. Revealing the structure within a complete ectodomain of the bent β knee is important for understanding the mechanism of integrin extension. Moreover, no bent integrin crystal structure to date has been described in light of current knowledge that this conformation occurs on cell surfaces and corresponds to the low-affinity state.
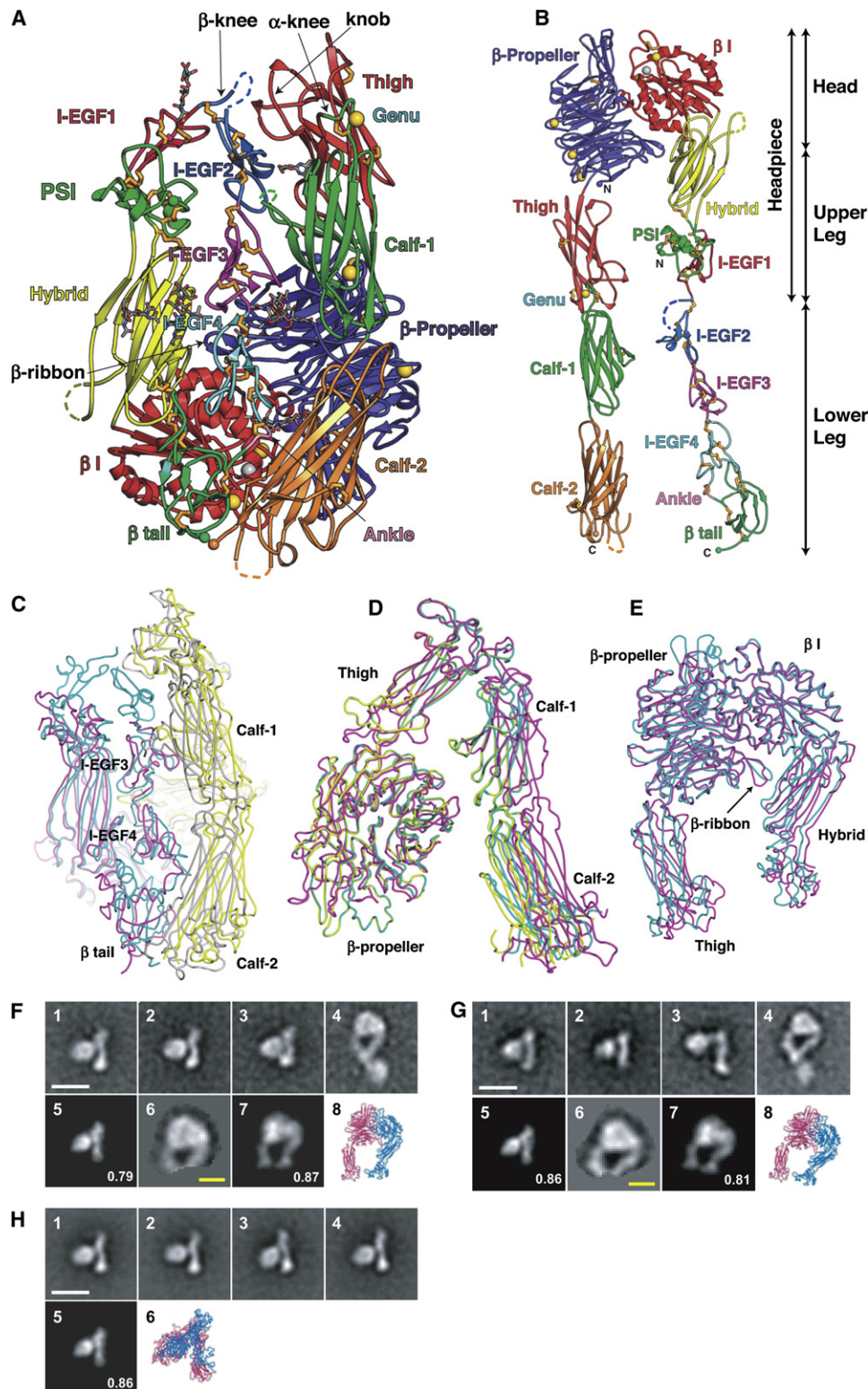
Figure 1. The $\alpha_{IIb}\beta_3$ Crystal Structure

(A) Cartoon diagram of molecule 1 in $\alpha_{IIb}\beta_3$ crystals. Ca and Mg ions are shown as gold and silver spheres, respectively. Disulfides are shown as gold sticks, and glycans are displayed as thinner sticks with gray carbons. C and N termini are shown as small spheres. Loops with missing density are shown as dashes.

(B) A model of $\alpha_{IIb}\beta_3$ extended by torsion at the α and β knees.

Most studies find that, upon activation, integrins extend (Luo et al., 2007). Upon extension, the headpiece can remain in the closed conformation, as when bent, or transition to an open conformation with high affinity for ligand, as shown in crystals of the $\alpha_{IIb}\beta_3$ headpiece bound to ligands (Xiao et al., 2004). In contrast, a "deadbolt model" posits that activation can occur in the absence of extension (Arnaout et al., 2005). Binding of cytoskeletal proteins such as talin and kindlins to the integrin β cytoplasmic domain appears to interfere with α/β cytoplasmic domain association and induce integrin extension (Wegener and Campbell, 2008). However, there is currently no known feature of integrin structure that would enable cytoskeleton binding to couple to the extended, open conformation with high affinity for ligand. This would appear to be important to fulfill the key role of integrins in integrating the extracellular and intracellular environments.

Three closely linked metal ion binding sites in the β I domain are especially important for ligand binding. Mg^{2+} at the central, metal-ion-dependent adhesion site (MIDAS) directly coordinates the acidic side chain shared by all integrin ligands. In previous unliganded, bent $\alpha_V\beta_3$ structures, the MIDAS and one adjacent site were unoccupied, and it was proposed that metal binding was either caused by integrin activation or induced by ligand binding (Xiong et al., 2002); however, crystals have not been reported with a combination of the two metal ions important for integrin ligand binding, Mg^{2+} and Ca^{2+}. Therefore, in current comparisons between low- and high-affinity β I domain conformations, the changes associated with ligand binding and metal binding cannot be deconvoluted.

Here, we describe the structure of platelet integrin $\alpha_{IIb}\beta_3$ in the bent conformation. Crystals with Ca^{2+} and Mg^{2+} show that, in the physiologic low-affinity state, the metal binding sites in the β I domain are fully occupied. Furthermore, the conformation is revealed of I-EGF domains 1 and 2 at the β knee, at the epicenter of conformational change. The arrangement of the legs within the bent structure and variation among structures in interdomain orientation have profound implications for the mechanism of integrin activation. Use of this information in models of extended integrins experiencing forces at sites of cell adhesion reveals how integrin affinity is regulated by force exerted parallel to the membrane by a motile actin cytoskeleton. Integrin structure and mechanochemistry provide a natural mechanism for increasing integrin affinity upon cytoskeleton attachment and decreasing it upon cytoskeleton disassembly.

RESULTS AND DISCUSSION

$\alpha_{IIb}\beta_3$ Crystal Structure and Negative-Stain EM

A 2.55 Å resolution crystal structure of the complete $\alpha_{IIb}\beta_3$ ectodomain with Ca^{2+} and Mg^{2+} has been refined to an R_{free} of 26.8% (Figure 1A and Table 1). In comparisons to $\alpha_V\beta_3$ below, differences in resolution and refinement should be kept in mind. The 3.1 Å $\alpha_V\beta_3$ structure is refined to an R_{free} of 36.7% (Xiong et al., 2004). $\alpha_{IIb}\beta_3$ has 95% and 0.4% residues in favored and outlier Ramachandran regions, respectively, and geometry in the 98th percentile (where 100 is the best), whereas $\alpha_V\beta_3$ has 76% and 6.7% residues in favored and outlier regions, respectively, and geometry in the 21st percentile, as reported by MOLPROBITY (Davis et al., 2007). Waters, which are important in hydrogen bonding and metal coordination, are in the $\alpha_{IIb}\beta_3$, but not the $\alpha_V\beta_3$ structure, as appropriate for their respective resolutions. No *cis*-prolines are present in the $\alpha_V\beta_3$ structure, whereas six are present in $\alpha_{IIb}\beta_3$. Two *cis*-prolines, Pro-163 and Pro-169, are in the ligand-binding β_3 I domain. The region around *cis*-Pro-169 has electron density typical for the $\alpha_{IIb}\beta_3$ structure (Figure S1 available online). There is a shift in the sequence-to-structure register between $\alpha_V\beta_3$ and $\alpha_{IIb}\beta_3$ at β_3 167–176, in the specificity-determining loop that forms the outer rim of the ligand-binding pocket in the β_3 I domain. Thus, the $\alpha_{IIb}\beta_3$ structure provides details about backbone conformation, hydrogen bonding, and side chain packing that are important for understanding ligand and metal binding, as well as for accurate molecular dynamics simulations and structure-guided mutagenesis. Furthermore, the structure factors for an integrin ectodomain have now been deposited, opening access to the experimental electron density upon which the atomic models are based.

Overall Bent Structure

The overall arrangement of domains in the two independent $\alpha_{IIb}\beta_3$ molecules in the asymmetric unit is similar to that in $\alpha_V\beta_3$ crystals (Figure 1C), except for differences in angles between domains (Table 2) that give insights into breathing. A similar bent conformation in solution with physiologic divalent cations is seen for three distinct $\alpha_{IIb}\beta_3$ constructs in negative-stain EM with class averaging (Figures 1F–1H and S2). The bent integrins from the three types of constructs are indistinguishable from one another (Figure 1F, panels 1–3, 1G, panels 1–2, and 1H, panels 1–4) and show excellent crosscorrelation with the $\alpha_{IIb}\beta_3$ crystal structure (Figure 1F, panels 1 and 5, 1G, panels 1 and 5, and 1H, panels 1, 5, and 6). One construct was clasped by appending to the α and β ectodomain C termini 15-residue linkers containing TEV

(C–E) Superpositions of molecules 1 and 2 of $\alpha_{IIb}\beta_3$ and $\alpha_V\beta_3$ (Xiong et al., 2004) showing breathing.

(C) A view showing variation in the distance of the lower α leg from the lower β leg, opening the cleft, and variation in the lower β leg. $\alpha_{IIb}\beta_3$ molecule 1 (α_{IIb}, gray; β_3, cyan) and $\alpha_V\beta_3$ (α_V, yellow; β_3, magenta).

(D) A view of the α subunit only, rotated about 90° from the view in (C), showing variation in the distance of the lower α leg from the upper α headpiece. $\alpha_{IIb}\beta_3$ molecule 1 (yellow) and molecule 2 (cyan); $\alpha_V\beta_3$ (magenta).

(E) The headpieces of $\alpha_{IIb}\beta_3$ molecule 1 (cyan) and $\alpha_V\beta_3$ (magenta), showing breathing at the β I/hybrid domain interface.

(F–H) Negatively-stained $\alpha_{IIb}\beta_3$ EM projection averages. Panels 1–4 show representative class averages. Panel 5 shows the 20 Å resolution-filtered $\alpha_{IIb}\beta_3$ crystal structure projection that best crosscorrelates with panel 1. Panel 6 in (F) and (G) shows the masked headpiece region from panel 4, and panel 7 shows the corresponding best-correlated $\alpha_{IIb}\beta_3$ headpiece crystal structure projection. Ribbon diagrams in panels 6 and 8 are in the same orientation (although enlarged) as the projections to their left. Numbers in panels 5 and 7 are normalized crosscorrelation coefficients. White and yellow scale bars are 100 and 50 Å, respectively.

(F) $\alpha_{IIb}\beta_3$ with a C-terminal coiled-coil clasp.

(G) $\alpha_{IIb}\beta_3$ with the clasp removed.

(H) $\alpha_{IIb}\beta_3$ disulfide-bonded near the C termini of the β tail and calf-2 domains.

Table 1. X-Ray Diffraction Data and Refinement

Protein	$\alpha_{IIb}\beta_3$ Ectodomain	$\alpha_{IIb}\beta_3$ Headpiece
Space group	P4$_1$	P6$_2$
Unit cell (a, b, c) (Å)	81.3, 81.3, 654.6	332.1, 332.1, 88.3
(α, β, γ) (°)	90, 90, 90	90, 90, 120
Wavelength (Å)	0.97934	0.9760
Resolution (Å)	50−2.55	45−2.90
Number of reflections (total/unique)	614,293/135,066	1,251,268/122,126
Completeness (%)	98.6/93.9[a]	98.3/93.9[a]
I/σ(I)	12.2/2.1[a]	17.4/3.0[a]
Rmerge (%)[b]	7.1/56.6[a]	9.7/60.2[a]
Rwork[c]/Rfree[d]	0.233/0.268	0.174/0.196
RMSD		
Bond (Å)	0.003	0.006
Angle (°)	0.736	0.659
Ramachandran plot[e]	95.0%/4.6%/0.4%	96.9%/2.9%/0.2%
PDB code	3FCS	3FCU (previously 1TYE)

[a] Numbers correspond to the last resolution shell.
[b] $R_{merge} = \Sigma_h \Sigma_i |I_i(h) - <I(h)>|/\Sigma_h \Sigma_i I_i(h)$, where $I_i(h)$ and $<I(h)>$ are the ith and mean measurement of the intensity of reflection h.
[c] $R_{work} = \Sigma_h||F_{obs}(h)| - |F_{calc}(h)||/\Sigma_h|F_{obs}(h)|$, where $F_{obs}(h)$ and $F_{calc}(h)$ are the observed and calculated structure factors, respectively. No I/σ cutoff was applied.
[d] R_{free} is the R value obtained for a test set of reflections consisting of a randomly selected 1.3% subset of the data set excluded from refinement.
[e] Residues in favorable, allowed, and outlier regions of the Ramachandran plot as reported by MOLPROBITY (Davis et al., 2007).

protease sites, followed by an α-helical coiled coil (Nishida et al., 2006). Association near the C termini of the α and β subunit ectodomains provided in vivo by association between the α_{IIb} and β_3 transmembrane domains (Luo et al., 2004) is mimicked by the clasp (Takagi et al., 2002). The clasped $\alpha_{IIb}\beta_3$ particles were 64% bent and 32% extended (with 4% unclassified) (Figure 1F). Unclasped particles, in which the clasp was removed with TEV protease, were 44% bent and 52% extended (Figure 1G). A third construct, which was identical to that used in crystallization, contained cysteines introduced in C-terminal portions of the α_{IIb} and β_3 subunits in positions that resulted in efficient disulfide bond formation in cell-surface integrins (Figure S3). The disulfide-bonded construct was 100% bent (Figure 1H).

The differing proportion of bent particles in the three preparations shows that tighter association near the C termini correlates with maintenance of the bent conformation and also with resistance to activation on the cell surface (Figure S3 and Supplemental Data). This is in agreement with work on other soluble integrin preparations and a large body of work on cell-surface integrins, which has shown that association of the α and β subunit transmembrane and cytoplasmic domains stabilizes integrins in the low-affinity state and in the bent conformation (reviewed in Luo et al., 2007).

Significance of the Bent Conformation

Similar bent conformations have previously been described in EM studies of the resting states of $\alpha_V\beta_3$, $\alpha_X\beta_2$, and $\alpha_L\beta_2$ (Nishida et al., 2006; Takagi et al., 2002). Furthermore, extensive studies using mutations and antibodies to ligand-induced binding sites (LIBSs) show that $\alpha_{IIb}\beta_3$ is compact on the cell surface when resting and extended when activated (Honda et al., 1995; Luo et al., 2007). The similarity in packing of two independent examples of $\alpha_{IIb}\beta_3$ and of $\alpha_V\beta_3$ in crystal lattices and similar appearance of multiple soluble integrins in EM, together with the work cited above, strongly suggest that the bent crystal structure determined here is representative of the resting state of most, if not all, integrins. However, three cryo-EM, EM, and hydrodynamic studies of detergent-soluble $\alpha_{IIb}\beta_3$ from platelets have reached conclusions that are incompatible with one another and with the domain arrangement seen here (Adair and Yeager, 2002; Rocco et al., 2008; Ye et al., 2008). The difficulty in obtaining a consensus view on $\alpha_{IIb}\beta_3$ structure may reflect the delicate equilibrium between bent and extended structures (Figures 1G and 1H), averaging over ensembles of bent and extended conformations, the poor association of the α_{IIb} and β_3 transmembrane domains in detergent (Wegener and Campbell, 2008), and dissociation of the heterodimer into the α_{IIb} and β_3 subunits (Carrell et al., 1985).

Conceptual advances since the previously described $\alpha_V\beta_3$ crystal structures allow us to describe the bent $\alpha_{IIb}\beta_3$ crystal structure in light of its physiological relevance as the low-affinity integrin state and as the starting point for integrin extension. Furthermore, the $\alpha_{IIb}\beta_3$ structure reveals I-EGF domains 1 and 2 and a highly acute bend between them in the bent conformation (Figure 1A). In contrast, I-EGF domains 2, 3, and 4 extend in an almost straight orientation, with an ∼90° left-handed twist between successive domains, to cover most of the length of the lower β leg (Figures 1A and 2A). The β knee, at the junction between I-EGF1 and I-EGF2, is flanked on one side by the PSI domain and on the other by a knob-like projection in the thigh domain (Figure 1A). The PSI and the knob are like goal post uprights, which define the passage for I-EGF1 and I-EGF2. The importance of the knob is emphasized by its structural conservation between α_{IIb} and α_V, in contrast to the flexibility of loops at the opposite end of the thigh domain, adjoining the β propeller domain (Figure 2D).

The I-EGF domains of the lower β leg are deeply buried in a narrow crevice between the upper β leg on one side and the upper and lower α leg on the other, with the β I and β propeller domains helping to form the back of the crevice (Figure 1A). The flexible calf-1 DX loop extends into the cleft and partially shields the lower β leg (Figures 1A and 2E). Exit of the lower β leg from the crevice appears to be the key step in integrin extension.

Overall Extended Structure

In the extended conformation, the α and β legs straighten at the knees and extend away from the headpiece (Figures 1F and 1G, panel 4). The closed headpiece from the crystal structure crosscorrelates excellently with the headpiece in EM (Figures 1F and 1G, panels 6–8), showing that, with Ca^{2+} and Mg^{2+}, extended $\alpha_{IIb}\beta_3$ predominantly assumes the closed headpiece rather than the open headpiece conformation (Figure 3A). Most extended class averages, whether with clasped or unclasped

Table 2. Variation in Interdomain Angles in Integrins[a]

Domain Interface	Bent $\alpha_{IIb}\beta_3$[b] Bent $\alpha_{IIb}\beta_3$	Bent $\alpha_{IIb}\beta_3$[c] Bent $\alpha_V\beta_3$	Bent $\alpha_{IIb}\beta_3$[d] Open $\alpha_{IIb}\beta_3$	Open $\alpha_{IIb}\beta_3$[e] Open $\alpha_{IIb}\beta_3$	Bent β_3[f] Frag β_2	Frag β_2[g] Frag β_2
α β propeller/α thigh	0.5°	9.7°–9.9°	—	—	—	—
α thigh/α calf1	1.3°	19°–20°	—	—	—	—
α calf1/α calf2	3.4°	14°–17°	—	—	—	—
β I/β hybrid	0.2°	6.7°–6.7°	58°–70°	1.2°–12°	—	—
β hybrid/β PSI	0.4°	7.2°–7.8 °	2.0°–11°	1.8°–9.2°	18°–27°	5.0°–8.3°
β PSI/β I-EGF1	0.8°	—	3.4°–13°	5.7°–18°	5.5°–40°	5.5°–41°
β hybrid/β I-EGF1	0.5°	—	6.8°–23°	11°–26°	29°–51°	3.7°–46°
β I-EGF1/β I-EGF2	0.4°	—	—	—	140°–170°	67°
β I-EGF2/β I-EGF3	1.2°	—	—	—	8.4°–8.5°	—
β I-EGF3/β I-EGF4	2.3°	5.4°–7.2°	—	—	—	—
β I-EGF4/β ankle	1.2°	10°–11°	—	—	—	—
β I-ankle/β TD	46°[h]	18°[i]	—	—	—	—
α β propeller/β I	0.2°	3.0°–3.3°	1.7°–2.8°	0.6°–1.1°	—	—

[a] Each pair of domains from two molecules was superposed using the first domain, and the change in angle upon superimposing the second domain was calculated. Dashes indicate where no comparison is possible, because only one or no domain pairs are available.
[b] Two molecules in current structure (1 × 1).
[c] Two molecules in current structure versus PDB code IU8C (2 × 1).
[d] Two molecules in current structure versus PDB 2VDR and three molecules in PDB 3FCU (2 × 4).
[e] Comparisons among 2VDR and three molecules in 3FCU (3 × 4/2).
[f] Two molecules in current structure and PDB 1U8C versus PDB 1YUK, PDB 2P26, and PDB 2P28 (3 × 3 to 3 × 1, depending on fragment length).
[g] Comparisons among PDB 1YUK, 2P26, and 2P28 (3 to 1 comparisons depending on fragment length).
[h] Residues common to molecules 1 and 2 in βTD are used, 606–612.
[i] $\alpha_{IIb}\beta_3$ molecule 1 compared to $\alpha_V\beta_3$.

$\alpha_{IIb}\beta_3$, show the α leg crossing over or under the β leg (Figures 1F and 1G, panel 4). Leg crossing appears to be a consequence of upper-leg configuration in the bent conformation with the long axis of I-EGF1 pointing toward the α knee (Figure 1A). When the bent crystal structure is extended at the α and β knees, leg crossing results (Figure S5A). However, the legs are highly flexible (see below) and, for clarity, are shown side by side in Figure 1B. Extended integrins with crossed and uncrossed legs have also been seen for activated $\alpha_V\beta_3$, $\alpha_X\beta_2$, and detergent-soluble $\alpha_{IIb}\beta_3$ integrins (Iwasaki et al., 2005; Nishida et al., 2006; Takagi et al., 2002).

After physiological activation of $\alpha_{IIb}\beta_3$ on platelets or treatment with high concentrations of ligands, multiple LIBS epitopes are exposed. These epitopes map to the lower β leg and to the PSI domain (Honda et al., 1995). The lower β leg is buried in a cleft in the bent conformation (Figure 1A) but will be exposed in the extended conformation (Figures 1B and S5A). Similarly, the LIBS epitope in the PSI domain, mapped to residues 1–6 (Honda et al., 1995), is masked by I-EGF2 in the bent conformation (Figure 1A). By contrast, this epitope is exposed after extension at the I-EGF1/I-EGF2 interface in the β knee brings I-EGF2 away from the PSI domain (Figure 1B). The previous functional studies, together with the location of these epitopes within the $\alpha_{IIb}\beta_3$ structure, demonstrate that bent and extended $\alpha_{IIb}\beta_3$ represent latent and activated integrins, respectively, contradict suggestions that $\alpha_{IIb}\beta_3$ is extended in the resting state (Rocco et al., 2008; Ye et al., 2008), and agree with electron tomography of active, detergent-soluble $\alpha_{IIb}\beta_3$, showing that it is extended (Iwasaki et al., 2005).

The Ligand-Binding Site Is Preloaded with Metals

Integrins bind ligands at the interface between the α subunit β propeller domain and β subunit I domain (Xiao et al., 2004; Xiong et al., 2002). These domains associate over an interface far larger than between other integrin domains (Table S1) to form the integrin head (Figures 1B and 3A). Three metal binding sites formed by loops in the β I domain underpin the ligand-binding site (Figures 3A–3C). Strong densities at all three sites reveal that they are occupied when physiologic divalent cations, Ca^{2+} and Mg^{2+}, are present (Figure 3C). Mg^{2+} at the central MIDAS site and Ca^{2+} at the two flanking sites are assigned by the coordination chemistry at these sites and the stronger electron densities at the two Ca^{2+} sites. In contrast, in previous $\alpha_V\beta_3$ crystals, in absence of ligand, only one divalent cation, either Mn^{2+} or Ca^{2+}, was present, and neither the ligand-associated metal binding site (LIMBS) nor MIDAS was occupied (Xiong et al., 2001, 2002).

Since our results show that the LIMBS is not a ligand-associated or -induced metal binding site, new nomenclature is required. We propose to rename this Ca^{2+}-binding site the synergistic metal ion binding site (SyMBS). Low concentrations of Ca^{2+} synergize with low concentrations of Mg^{2+} for ligand binding to integrins (Marlin and Springer, 1987), and mutational studies show that the SyMBS has a positive regulatory effect on ligand binding and that the SyMBS is the site responsible for Ca^{2+} synergy (Chen et al., 2003; Mould et al., 2003). The SyMBS designation also honors the finding with $\alpha_V\beta_3$ crystals that ligand binding at the MIDAS synergizes with Mn^{2+} binding at the SyMBS when Ca^{2+} is absent (Xiong et al., 2002).
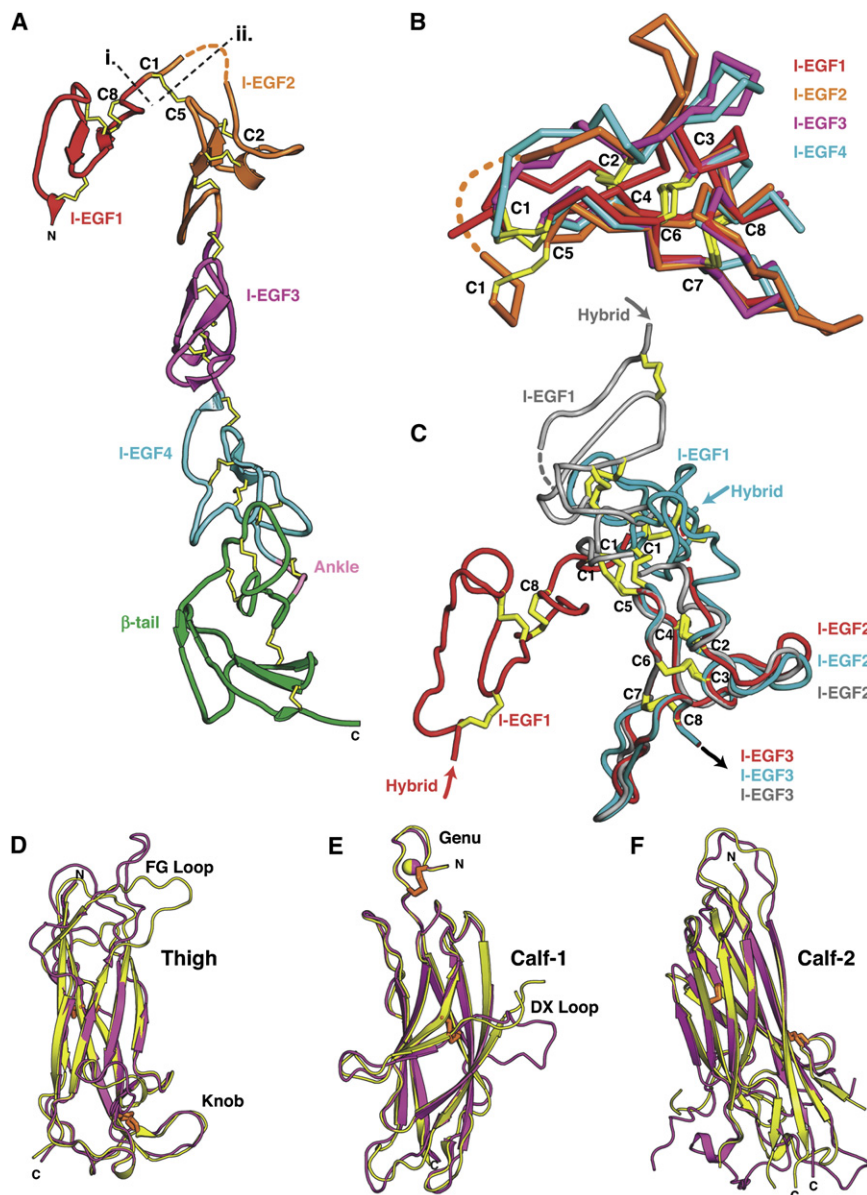
Figure 2. Integrin Leg Domains

(A) The knee and lower β leg of $\alpha_{IIb}\beta_3$. Dashes mark gimbal flexion positions.

(B) Superposition using SSM (Krissinel and Henrick, 2004) of $\alpha_{IIb}\beta_3$ I-EGF domains 1–4 in the same color scheme as in (A).

(C) Superposition using I-EGF2 of I-EGF 1 and 2 module pairs. Domains from $\alpha_{IIb}\beta_3$ are in red, and those from β_2 fragments (Shi et al., 2007) are in cyan and gray.

(D–F) Superposition of α_{IIb} (yellow) and α_V (magenta) (Xiong et al., 2004) thigh (D), calf-1 (E), and calf-2 (F) domains.

MIDAS. Furthermore, the SyMBS site is completely buried and would be difficult to occupy after ligand binding.

The major differences between low- and high-affinity ligand-binding site conformations are the movements of the β1-α1 loop and its bound adjacent to MIDAS (AdMIDAS) Ca^{2+} toward the MIDAS Mg^{2+}, as previously described (Xiao et al., 2004; Xiong et al., 2002) (Figures 3C–3E). In a similar movement of the β1-α1 loop in α I domains, the MIDAS metal ion moves 2 Å away from an Asp and toward a Thr in the high-affinity state and thus becomes more electrophilic for the acidic ligand residue (Arnaout et al., 2005; Luo et al., 2007) (Figure 3F).

The current structure enables comparison of MIDAS metal ion and water positions between the low- and high-affinity states of β I domains. Our structure reveals that, in contrast to α I domains, there is no lateral movement of the MIDAS metal ion across the ligand-binding pocket (Figures 3E and 3F). In α I domains, the second Ser of the DXSXS motif (α_L Ser-141 in Figure 3F) moves to the position of the Mg^{2+} ion and pushes the Mg^{2+} toward Thr-206 in the high-affinity conformation (Figure 3F). In β I domains, the Mg^{2+} is already in a ligand-binding position in the low-affinity state, and the second Ser of the DXSXS motif, Ser-123, moves toward the Mg^{2+} from secondary coordination and displaces a water to occupy the primary coordination sphere (Figures 3C–3E).

What then is the basis for the increase in affinity of β I domains in the open conformation? In part, this must be due to the movement toward the MIDAS of the β1-α1 loop bearing the DXSXS motif, enabling two of its backbone N atoms to form stabilizing hydrogen bonds to the two O atoms of the ligand Asp side chain (Figure 3D). Additionally, movement in the open state of the AdMIDAS Ca^{2+} toward the MIDAS brings it into primary coordination with Asp-251, enabling Asp-251 to polarize toward the AdMIDAS Ca^{2+} (Figure 3D) rather than toward the MIDAS Mg^{2+} (Figure 3C). Furthermore, there is a significant increase of 1 Å

Figure 3C reveals the structural basis for synergy between the SyMBS and MIDAS. Although coordination at the MIDAS is octahedral, with six ligands, four of these are waters. An unusually low number of two Mg^{2+} oxygen ligands come from protein, donated by the side chains of β_3 Ser-121 and Glu-220. The side chain of Glu-220 orients between the SyMBS and MIDAS, with one oxygen coordinating the SyMBS Ca^{2+} and the other coordinating the MIDAS Mg^{2+} (Figure 3C). In the absence of either of these metals, the Glu-220 would likely reorient and not form a proper coordination to the other site, explaining the basis for synergy.

It is conceptually attractive to find that the physiologically important metals Ca^{2+} and Mg^{2+} are preloaded prior to ligand binding. The Asp side chain of integrin ligands such as Arg-Gly-Asp (RGD) directly coordinates the MIDAS Mg^{2+} (Figure 3D). In the absence of Mg^{2+}, approach of this Asp would be electrostatically repelled by Glu-220, Asp-119, and Asp-251 around the
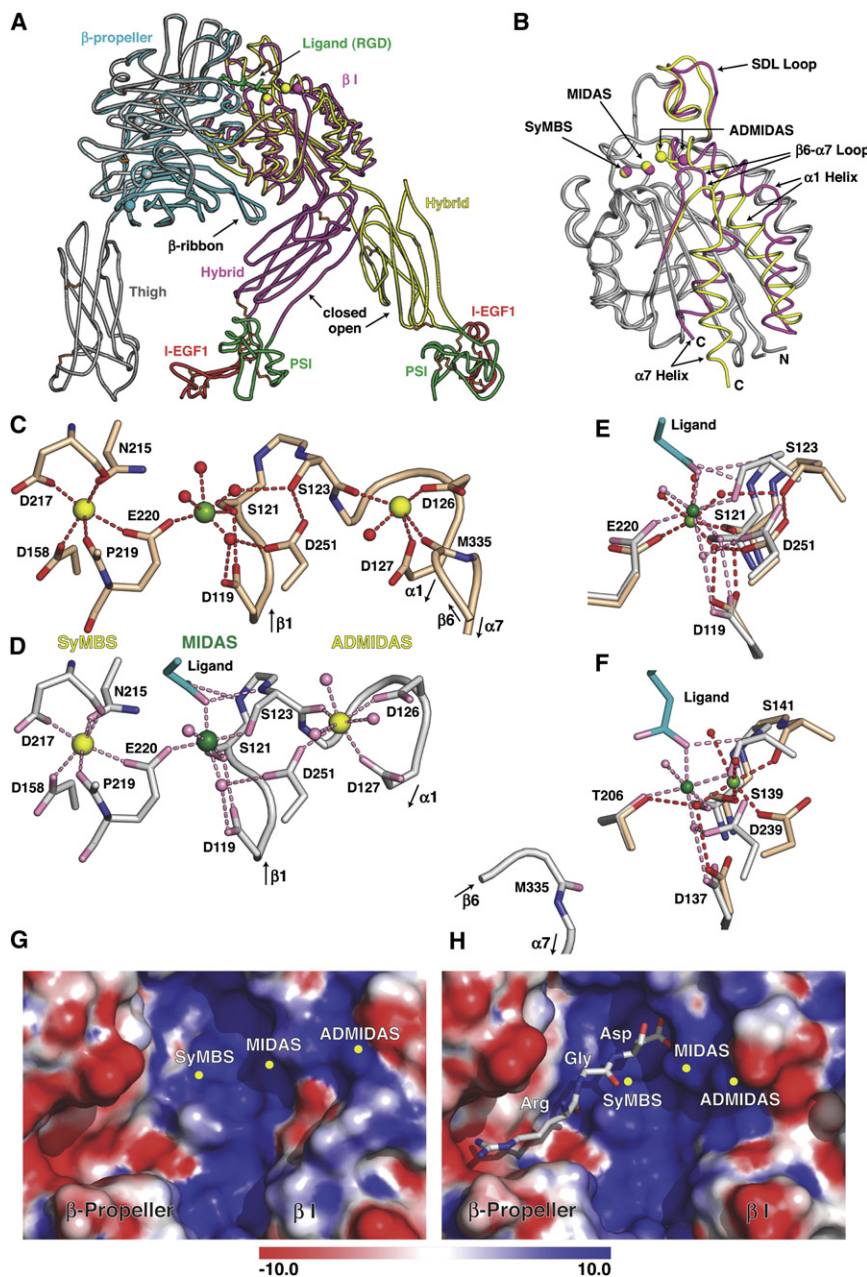
Figure 3. Metal Ion Rearrangements in β I Domain Activation

(A) Superposition of headpieces from our unliganded-closed structure and liganded-open $\alpha_{IIb}\beta_3$ (Springer et al., 2008). The β I and hybrid domains are yellow (open) and magenta (closed), while PSI and I-EGF1 domains are red and green, respectively. The α headpieces are cyan (open) and gray (closed).

(B) Enlarged view of β I domains with major differences in yellow (open) and magenta (closed).

(C and D) β I domain metal coordination sites in unliganded-closed $\alpha_{IIb}\beta_3$ (C) and liganded-open $\alpha_{IIb}\beta_3$ (D). Ca (gold) and Mg (green) ions are large spheres; waters (red or pink) are smaller spheres. N atoms are blue and O atoms are red or pink. Metal coordination and hydrogen bonds are dashed. The loop bearing M335 moves far away in (D).

(E) Superposition at the β I MIDAS.

(F) Superposition at the α I MIDAS of unliganded-closed (PDB code 1LFA) and liganded-open α_L (PDB code 1T0P) in the same orientation as the β I MIDAS in (D). In (C)–(F), carbons for unliganded-closed and liganded-open integrins and for ligands are wheat, gray, and cyan, respectively.

(G and H) Electrostatic potential surfaces at the unliganded (G) and liganded (H) binding sites.

et al., 2002; Shi et al., 2007). As shown below, the disulfides are compatible with large interdomain rearrangements, and there is no need for disulfide reduction for integrin activation as previously suggested (Yan and Smith, 2001).

Integrin EGF Domains

Eight cysteines are disulfide bonded in a C1-C5, C2-C4, C3-C6, and C7-C8 pattern in the small, 37–50 residue I-EGF domains (Figure 2B). The exception is I-EGF1, which lacks the C2-C4 disulfide. This enables the C1-C3 loop to occupy a position different than in other I-EGF domains (Figure 2B) and prevents clashes and enables greater flexibility at interfaces with the PSI and I-EGF2 domains.

in separation between the Mg^{2+} and Asp-119 in the open state (Figure 3E and Supplemental Data). The backbone, AdMIDAS, and Asp-119 movements all increase the positive potential in the environment of the MIDAS and promote greater electrophilicity of the Mg^{2+} for ligand in the high-affinity, open state. The overall increase in positive potential near the MIDAS in the high-affinity state is apparent in electrostatic potential surfaces (Figures 3G and 3H).

The Flexible β Knee and β Leg

The structure shows that all 56 cysteines in the integrin β_3 subunit are disulfide bonded, and the disulfides exhibit no rearrangements with respect to integrin fragment structures (Beglova

The connection between tandem I-EGF domains is gimbal-like, since two flexion points are revealed at the highly acute bend between I-EGF1 and I-EGF2 at the β knee (Figure 2A, dashed lines). Between tandem I-EGF domains and also at the PSI/hybrid and hybrid/I-EGF1 junctions, only one residue intervenes between the last Cys of one domain and the first Cys of the next, limiting flexion at this C-X-C junction (Figure 2A, dashed line "i"). However, the disulfide unique to I-EGF domains between C1 at the N terminus and C5 in the β hairpin turn between the two β strands (Figures 2B and 2C) is surprisingly flexible. Most of the movement at the β knee occurs at a second point of flexion within the tip of I-EGF2, in the C1-C5 disulfide and in the disordered loop connecting C1 and C2 (Figure 2A, dashed line "ii"). This is evident

from superpositions of β3 I-EGF domains 1–4 (Figure 2B) and β2 leg fragments (Figure 2C). The position of C1 is highly variable in these superpositions, demonstrating flexibility of the N-terminal tip of the I-EGF domain, particularly in I-EGF2. Although previous examples of I-EGF1/I-EGF2 interfaces in β2 leg fragments had been termed bent and extended (Shi et al., 2007), the two fragments differ in angle by 140° to 170° from I-EGF1/I-EGF2 in $\alpha_{IIb}\beta_3$, and both are extended compared to the highly bent conformation revealed here (Table 2 and Figure 2C). Thus, the gimbal-like connection between I-EGF domains is permissive of extreme rotations and a wide range of interdomain orientations.

A corollary to the gimbal-like junction at I-EGF domains is that flexibility should be related to the length and disorder of the polypeptide chain between C1 and C2 (or between C1 and C3 in I-EGF1, which lacks the C2-C4 disulfide). As fitting for its role in extension of the β leg, the C1-C2 loop of I-EGF2 is the only disordered I-EGF loop in our structure and is located at the apex of the β knee (Figures 1A and 2A). Furthermore, alignment of integrin β subunits β1–β8 in diverse vertebrates shows that I-EGF2 has the longest C1-C2 loop, with 9 to 13 residues. By contrast, the C1-C2 loop has 4 residues in I-EGF3 and 6–7 residues in I-EGF4. In I-EGF1 the 8–10 residue length of the C1-C3 loop is consistent with variations of up to 41° at the PSI/I-EGF-1 junction in comparisons to $\alpha_{IIb}\beta_3$ headpiece and β_2 leg fragments (Table 2 and Figure S7). Furthermore, disorder of I-EGF1 and I-EGF2 in the $\alpha_V\beta_3$ crystal structure (Xiong et al., 2001) implies flexibility at the PSI/I-EGF1 and I-EGF2/3 interfaces.

The β Ankle

A disulfide-bonded loop between I-EGF4 and the β tail domain, previously defined as part of I-EGF4, has no equivalent in other EGF domains and is termed here the β ankle. It is not integrated by backbone hydrogen bonds into I-EGF4 or the β tail and is likely to be flexible in extended integrins.

The β Tail

Flexibility between the β ankle and β tail is substantial, with up to 46° variation (Table 2). Flexibility within the N-terminal α helix of the β tail is suggested by loss of density in molecule 2 midway through this helix and by the weak density of the β tail domain in molecule 1. The better order of the β tail in $\alpha_V\beta_3$ appears due to an unusually large lattice contact of 860 Å², which is larger than any domain-domain junction within the β knee or lower β leg (400–550 Å²) (Table S1).

A contact between the CD loop of the β tail domain (termed the "deadbolt") and the α7 helix of the β I domain has been proposed to inhibit integrin activation (Arnaout et al., 2005), although the size of this interface at 60 Å² is too small to be significant (Janin, 1997). There is no such contact in $\alpha_{IIb}\beta_3$, either in molecule 1, where the orientation of the β tail differs, or in molecule 2, where this part of the β tail is disordered. Since the β I domain in both molecules is in the inactive, closed conformation, the CD loop does not act as a deadbolt to restrain integrin activation. In agreement, mutation or deletion of the CD loop has no effect on activation of cell-surface $\alpha_V\beta_3$ or $\alpha_{IIb}\beta_3$ integrins (Zhu et al., 2007a).

Integrin Breathing and Extension
Breathing in the Bent Conformation

In molecule 2 of $\alpha_{IIb}\beta_3$ compared to molecule 1, the lower α leg swings outward at the genu, away from both the upper α and

β legs, thus widening the crevice in which the lower β leg is buried (Figure 1D). The I-EGF4 and β tail domains also swing with the α leg away from the upper β leg. In $\alpha_V\beta_3$ crystals, the lower α leg swings out further, and the I-EGF domains 3 and 4 in the lower β leg move away from the hybrid domain in the upper β leg (Figures 1C and 1D). About 10% of $\alpha_V\beta_3$ and $\alpha_{IIb}\beta_3$ particles exhibit substantially more opening between the lower legs and headpiece than other particles (Figure 1G, panel 3) (Takagi et al., 2002). This opening is similar in directionality but greater in amplitude than in the crystal structure comparisons.

A second component of breathing motion is swinging of the hybrid domain relative to the β I domain. The hybrid domain is more swung out in $\alpha_V\beta_3$ than in $\alpha_{IIb}\beta_3$ (Figure 1E) and has a smaller interface with the β I domain. Swinging opens the crevice in which the lower β leg is buried and has the same directionality as transit to the open headpiece.

A flexible β ribbon extension of the β2-β3 loop of β propeller blade 5 (Figure 1A) also evidences breathing. It differs in position between $\alpha_V\beta_3$ and $\alpha_{IIb}\beta_3$ (Figure 1E) and between $\alpha_{IIb}\beta_3$ structures (Figure 3A). An introduced disulfide bond between the β ribbon and I-EGF4 stabilizes $\alpha_V\beta_3$ and $\alpha_{IIb}\beta_3$ in the bent conformation and prevents integrin activation on cell surfaces (Takagi et al., 2002). The residues mutated to cysteine are close in $\alpha_V\beta_3$ and not in $\alpha_{IIb}\beta_3$, demonstrating that the β ribbon can differ significantly in position in bent $\alpha_{IIb}\beta_3$ (Supplemental Data).

The main components of motion, hinging of the legs and swinging of the hybrid domain, provide a plausible pathway for integrin extension. Each of these components is confirmed to be a low-frequency and, hence, important normal mode (data not shown). Both types of motions will allow release of the lower β leg from its crevice between the upper β leg and lower α leg (Figure 1A).

Extension

After release of the lower β leg, the highly flexible I-EGF1/I-EGF2 interface could transit from its bent to extended conformation while, at the same time, extension occurs at the α-genu, resulting in a switchblade-like opening of the integrin. Flexibility described above at the PSI/I-EGF1, I-EGF1/I-EGF2, and β ankle/β tail interfaces is also important to enable the lower α and β legs to extend without clashing near the knees, where the long axis of I-EGF1 points toward the α knee (Figure 1A). Reorientation of the ligand-binding head so that it points away from, rather than toward, the cell surface and extends further above it will greatly facilitate ligand binding (Figure 1B). Furthermore, extension frees the hybrid domain from extensive interfaces in the bent conformation (Table S1), making hybrid domain swing-out to the open conformation less energetically costly. However, it is sterically possible for hybrid domain swing-out to occur simultaneously with, or precede, extension.

Integrin Ectodomain Structure Provides a Mechanism for Force-Induced Integrin Activation and Deactivation

Binding of the actin cytoskeleton-associated proteins talin and kindlins to specific residues in the integrin β subunit cytoplasmic domain is crucial for inside-out activation of integrins and bidirectional signal transmission (Moser et al., 2008; Wegener and Campbell, 2008). Talin and kindlins bind through their FERM domains to distinct NPX(Y/F) motifs in integrin β subunit

cytoplasmic domains that are membrane proximal and distal, respectively. Talin binding to the β subunit cytoplasmic domain has been proposed to sterically interfere with α and β subunit cytoplasmic domain association. One model is that talin binding would alter the depth in the membrane of the β subunit transmembrane domain or its angle with respect to the α subunit transmembrane domain. Another model is that talin binding would cause dissociation of the α and β subunit transmembrane domains, i.e., separation in the membrane (Luo et al., 2004; Wegener and Campbell, 2008). However, steric interference with α and β subunit association is more difficult to envision for kindlins, which bind to a membrane-distal motif that is disordered in αβ cytoplasmic complexes (Wegener and Campbell, 2008).

Crosslinking the integrin α and β subunit transmembrane domains and fluorescence resonance between probes attached to the cytoplasmic domains have each demonstrated that both inside-out and outside-in signaling require separation of the α and β subunit transmembrane domains and are associated with separation of the cytoplasmic domains (Luo et al., 2007). Transmembrane and cytoplasmic domain separation would lead to separation of the lower α and β legs, which, in turn, would destabilize their interfaces with the head and upper legs and trigger integrin extension. However, extended integrins can have either the closed or open headpiece with low or high affinity for ligand, respectively. This begs the question of whether the open, high-affinity headpiece conformation could be enforced by signals within the cell. The complete integrin ectodomain structure described here now allows an analysis of how force is transmitted between the ligand-binding site and the transmembrane domains to regulate transition between low- and high-affinity states.

There is great interest in the concept that force is important in regulating the adhesiveness and conformation of integrins (Alon and Dustin, 2007; Astrof et al., 2006; Evans and Calderwood, 2007; Puklin-Faucher et al., 2006). However, a key factor that has not previously been considered is the lateral force exerted by actin cytoskeleton treadmilling or contraction. Talin and kindlins link integrins through a molecular clutch to the actin cytoskeleton. As a consequence, integrins move laterally on the cell surface at speeds of up to 130 nm/s in the same direction as actin filaments (Hu et al., 2007; Kaizuka et al., 2007). Thus, integrin binding to talin and kindlins is essentially synonymous with attachment to the cytoskeleton and exertion of a lateral force on the β subunit cytoplasmic domain.

Let us envision at the molecular level the consequences of dragging an integrin by its β tail across the cell surface. Bent integrins have a cross-section of 80 × 100 Å near the plasma membrane that is unusually large for a cell-surface glycoprotein. The dense packing of extracellular domains on the cell surface is one of the major barriers to diffusion (Sheetz, 1993). Thus, as an integrin is dragged across the cell surface, it would be buffeted by collisions with other cell-surface glycoproteins. The thin, lower β leg is shielded in its cleft by the robust α subunit and upper β leg and head (Figure 1A), which will bear the brunt of buffeting. Thus, the integrin will be forced through a gauntlet of other cell-surface proteins that will strip the α subunit and upper β leg away from the lower β leg that they shield. Furthermore, the calf-2 domain has an unusually broad base for a cell-surface domain and two long unstructured loops near the plasma membrane,

one of which is cleaved during biosynthesis (Figure 2F). Frictional forces due to interactions of these segments and the α subunit transmembrane domain with the plasma membrane will also pull the α leg away from the β leg.

These forces are on pathway with the breathing movements described above and will shift the equilibrium toward integrin extension. Although the interfaces buried in the bent conformation are extensive (Table S1), they have low shape complementarity, are mainly hydrophilic, and are readily replaced by water, as shown by the shift in equilibrium toward extension upon C-terminal clasp cleavage (Figures 1F–1H) (Nishida et al., 2006; Takagi et al., 2002). Because of the central role of the lower β leg in these interfaces (Table S1 and Figure 1A), its removal from the cleft will destabilize the bent conformation far more than clasp removal and result in extension. Furthermore, extension places the bulky head of the integrin above the height of most cell-surface glycoproteins, reducing frictional drag and favoring maintenance of extension.

Once the integrin is extended, lateral pulling on β will align the integrin so that β orients toward and α away from the pulling direction. Orientation will be enhanced by frictional resistance of the three leg domains in α, which, at 140–170 residues and with extra β strands compared to Ig domains, are unusually stout (Supplemental Data) and will act as a sea anchor. In contrast, β leg domains are at the lower size limit found on cell surfaces.

Extended and not bent integrins are competent for binding large biological ligands such as fibronectin and fibrinogen (Zhu et al., 2007a). Once a ligand in the extracellular matrix or on the surface of another cell is bound, resistance to lateral pulling by the β subunit cytoplasmic domain will increase greatly, with a corresponding increase in the lateral force. Because the β subunit hybrid domain extends laterally away from the ligand-binding site in the open headpiece conformation (Figure 3A), the lateral force should stabilize the open headpiece conformation.

To test how forces regulate the conformation of the integrin headpiece, we used the complete ectodomain structure and the liganded, open headpiece structure (Springer et al., 2008; Xiao et al., 2004) to build extended integrin models with the headpiece closed or open and bound to the specific peptide recognition motif in fibrinogen (Figures 4A and 4D). The C termini of the α and β subunit ectodomains were tethered to a plane to mimic the plasma membrane. To mimic a cell pulling away from ligand in matrix or on the surface of another cell, a tensile (pulling) force normal to the membrane was applied to the α and β ectodomain C termini (Figures 4C and 4F). Since the ligand remained stationary, over time, an equal and opposite resisting force built up on it (Figures 4C and 4F). This mimics forces experienced by the integrin and ligand during cell adhesion in the absence of attachment of the integrin to the cytoskeleton. Alternatively, the same membrane-normal forces were applied, and an additional lateral force parallel to the membrane was applied to the C terminus of the β subunit ectodomain that was resisted by the stationary ligand (Figures 4B and 4E). This mimics forces experienced during cell adhesion in the presence of attachment of the integrin β subunit to talin or kindlins and the actin cytoskeleton.

In the presence of both the membrane-normal force exerted by ligand and the lateral force exerted by the cytoskeleton, the
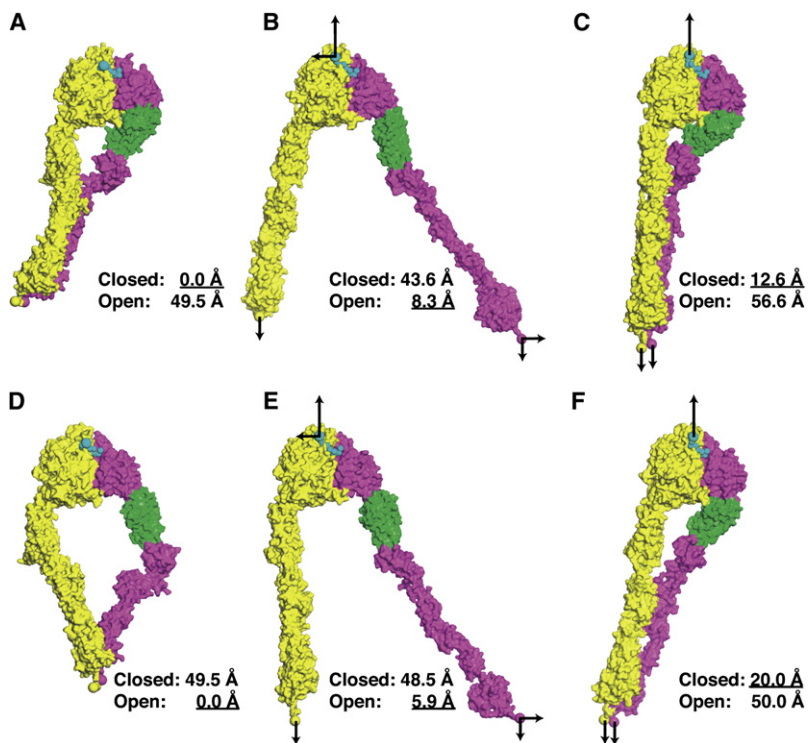
Figure 4. Regulation of Integrin Conformation by Tensile Force

Molecular surfaces show α_{IIb} in yellow and β_3 in magenta with hybrid domain in green. Fibrinogen peptide ligand is shown in cyan as $C\alpha$ spheres. (A) and (D) are starting models. (B) and (C) are derived from (A), and (E) and (F) from (D) after applying tensile forces (arrows) in steered molecular dynamics simulations to α_{IIb} and β_3 C-terminal and ligand N-terminal atoms shown as large spheres. Models in (A–F) are aligned by superposition on the β propeller and β I domains. Numbers show the distance after superposition of C-terminal residue 433 of the hybrid domain from the closed (A) and open (D) conformations. The underlined distance shows the conformation that models most closely resemble.

explaining the structural basis for inside-out signaling (Figure 5). New sites of attachment of integrins to matrix are formed in the lamellipodium, where actin polymerization and branching is rapid (Broussard et al., 2008; Choi et al., 2008). Actin filaments in this region actively move backward toward the lamella. Integrins that associate with the actin cytoskeleton move rapidly along the cell surface, as observed with nanobeads (Giannone et al., 2003), and would be extended by the frictional buffeting forces described above (Figure 5B). Once the integrins bind ligand, the ligand will resist the pulling force, increase the lateral tensile force, and thereby stabilize the high-affinity state (Figure 5C). Moreover, there is a positive feedback loop, because ligand binding reinforces integrin attachment to the cytoskeleton and is important in the maturation of nascent adhesions (Broussard et al., 2008; Giannone et al., 2003). Thus, firm adhesion to the matrix is established at sites in the lamellipodium where actin polymerization occurs and contact with ligand is made, further reinforcing attachment between integrins and the cytoskeleton. This provides traction near the lamellipodium to support further protrusion of the leading edge of the cell. As new membrane is added and the cell moves forward, the nascent adhesion sites will be left behind and find themselves in the lamella. Here, double-headed myosin II is present, which contracts actin filaments, and nascent adhesions can mature to focal adhesions or disassemble (Broussard et al., 2008; Choi et al., 2008).

For cell migration, detachment at the rear of the cell is just as important as adhesion at the leading edge. When integrins are artificially locked in the high-affinity state or actin disassembly in the uropod is blocked with rho kinase inhibitors, uropod retraction is blocked and cells become highly elongated and stop migrating (Smith et al., 2007). As cells migrate over a substrate, the integrins that remain bound to ligand on the substrate will eventually find themselves in the uropod. Cytoskeleton disassembly in the uropod is coordinated with destabilization of adhesions (Broussard et al., 2008). In the absence of a lateral force on the β subunit, the normal force exerted on the integrin as the uropod pulls away from ligand stabilizes the closed headpiece with low affinity for ligand (Figure 5D). This favors ligand dissociation (Figure 5E). The integrin can, thus,

extended-open integrin remained open (Figure 4E). In the case of the extended-closed integrin, the lateral force was transmitted through the lower β leg domains to the hybrid domain, which swung out and assumed an orientation similar to that in the open headpiece (Figure 4B). Thus, binding to the actin cytoskeleton provides an active mechanism for separating the integrin α and β legs and inducing the extended-open integrin conformation with high affinity for ligand at sites of actin polymerization and contraction.
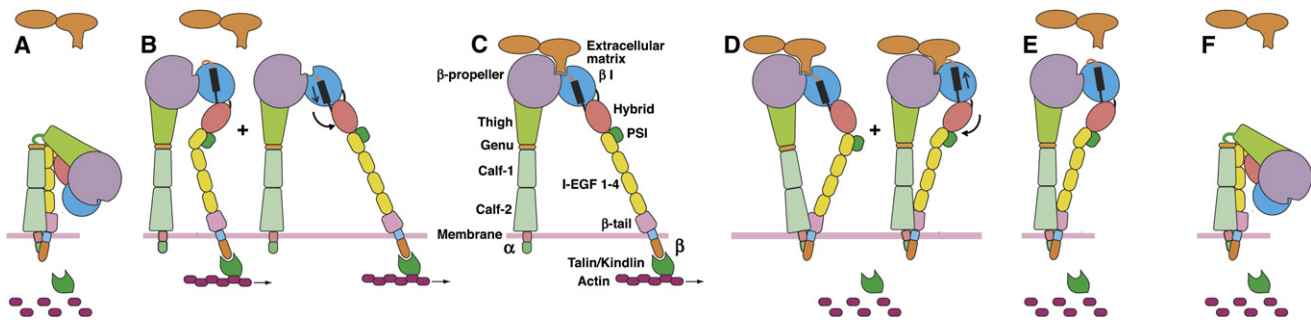
In the presence of only the force pulling the integrin away from ligand, the α and β legs remained together and were extended (Figures 4C and 4F). The closed-extended integrin remained closed (Figure 4C). In the case of the open-extended integrin, the greater leg extension induced by tensile force caused the hybrid domain to swing inward toward the closed headpiece conformation (Figure 4F). Thus, a tensile force exerted on the ligand-integrin complex in the absence of cytoskeleton engagement stabilizes the closed, low-affinity state of the headpiece, opposite to previous expectation (Alon and Dustin, 2007). Thus, force-induced stabilization of the low-affinity state provides an active mechanism for downregulating integrin adhesion in migrating cells at sites of actin cytoskeleton disassembly, including the uropod, and enables integrins and plasma membrane to be internalized for transport in intracellular vesicles toward the front of the cell (Broussard et al., 2008).

Implications for Integrin-Mediated Cell Adhesion and Migration

The above results show that inherent in integrin structure is a mechanism for activating the ectodomain by attachment of the actin cytoskeleton to the β subunit cytoplasmic domain,

Figure 5. The Integrin Cycle

(A) In the bent conformation, integrins have low affinity for ligand.

(B) At sites where actin filaments are formed, the integrin β subunit cytoplasmic domain binds through talin or kindlins. Lateral translocation on the cell surface and buffeting cause integrin extension. Both open and closed headpiece conformations are putatively present.

(C) Binding to an immobilized extracellular ligand greatly increases the lateral force and markedly favors the high-affinity, open headpiece conformation.

(D) Disassembly of the actin cytoskeleton removes the lateral force. Tensile force between the ligand and the integrin cytoplasmic domains favors the closed headpiece conformation and ligand dissociation.

(E) Ligand dissociates, further favoring the closed headpiece conformation.

(F) In the absence of ligand and tensile force, the bent conformation is favored, completing the cycle, and the integrin returns to the same state as shown in (A).

return to the low-affinity, bent conformation, completing the integrin adhesion/detachment cycle (Figure 5F).

Activation of the high-affinity state by the lateral pull exerted by the actin cytoskeleton provides an elegant solution to the problem of coordinating ligand binding by integrins to attachment to the cytoskeleton. The importance of the cytoskeleton for integrin function is supported by many studies. For example, actin cytoskeleton-disrupting agents inhibit integrin adhesion stimulated by inside-out signaling, i.e., affinity regulation (although not avidity regulation) (Kim et al., 2004). Actin filament movement is highly coordinated with movement of ligand-bound integrins into the ring-shaped immunological synapse, and actin poisons rapidly disperse integrins, but not other adhesion molecules, from the synapse (Kaizuka et al., 2007).

Our simulations used comparable forces normal and lateral to the cell surface as might be found in the lamellipodium; however, in focal contacts where actin stress fibers terminate, the lateral force exerted on the β tail by the cytoskeleton may be much greater than the normal force. This would only increase the tendency of lateral force to stabilize the open headpiece conformation with high affinity for ligand. In geometries in which no force is applied to the α tail, applying tensile force to the β tail alone will stabilize the high-affinity state, since, in the open headpiece, the β subunit is much more extended than in the closed headpiece, with distances between the ligand-binding MIDAS in the β I domain and C terminus of the hybrid domain of 83 and 64 Å, respectively (Astrof et al., 2006). In typical representations, integrins extend approximately normal to the cell surface (Figure 5). However, the direction of integrin extension will be determined by the force vectors. When lateral force is stronger than normal force, integrins will extend more in the direction parallel than normal to the membrane, i.e., they will lean over. Such a change in integrin orientation is consistent with measurements of cell-substrate distances by interference reflection microscopy and EM (Verschueren, 1985). The height to which integrins extend above the surface of 200–250 Å in our simulations is similar to the distance of 300 Å between the plasma membrane and extra-

cellular matrix at close contacts in the lamellipodium of migrating cells. However, a membrane-matrix distance of 100–150 Å is found at focal contacts, consistent with an extended, leaned-over integrin conformation in the presence of strong lateral force.

We believe that application of lateral force is the most physiologically relevant mechanism for activating integrins, but not the only one. Separation of the transmembrane and cytoplasmic domains, in the absence of an applied force, appears sufficient to induce integrin extension. This should enable at least a small fraction of integrins to transition to the extended-open conformation and may be sufficient for integrin adhesiveness in many commonly employed assays. Disruption of association between membrane-proximal cytoplasmic regions may be sufficient to induce extension and may explain why deletion of either the integrin α or β subunit cytoplasmic domains is activating (Lu et al., 2001; Lub et al., 1997). However, in contrast to other activation mechanisms, association with the actin cytoskeleton uniquely enforces selection of the extended-open conformation over the bent and extended-closed conformations and selectively enhances the adhesiveness of those integrins that are experiencing tensile forces as a consequence of simultaneous binding to ligand and the cytoskeleton (Figure 5C). Thus, this mechanism exquisitely supports the function of integrins in integrating cell adhesion and cell migration.

The mechanism described here is mechanochemical, since force alters the chemical equilibrium between conformational states and drives integrins from a bent, closed headpiece, low-affinity state to an extended, open headpiece, high-affinity state. The mechanism is also allosteric, with force as the allosteric effector. Previously, it has not been thought possible to transmit signals through flexible protein domains, because allostery involves relative changes in orientation and position and flexibility decouples the relative positions of sending and receiving domains. However, tensile force extends and imparts stiffness to flexible proteins and, thus, enables signal transduction through otherwise flexible protein regions. The outward swing of the hybrid domain, and with it the PSI domain in the upper β leg,

transmitted through stiffened β knee and β leg domains, elegantly couples rearrangements at the ligand-binding site in the β I domain to lateral force exerted by the actin cytoskeleton.

The integrin mechanochemical mechanism works well whether talin or kindlins link integrins to actin microfilaments that are moving as a consequence of myosin contraction, extension/polymerization at the leading edge, or treadmilling. This mechanism would not work for reception of signals from soluble ligands but is uniquely well suited for adhesion receptors. This structural mechanism for linking cytoskeleton binding to ligand binding appears to be at the heart of the integrating function that gives integrins their name and enables them to provide the traction for cell migration. Outside-in signaling by integrins requires both α and β subunit transmembrane domain separation and clustering (Miyamoto et al., 1995; Zhu et al., 2007b). Cytoskeleton association may contribute to both of these components, first by inducing transmembrane domain separation and second by cooperating with binding to multivalent ligands in inducing clustering.

Undoubtedly, further levels of complexity are added by the many members of the integrin family, including the distinctive β4 subunit; the large number of proteins that interact with integrin β cytoplasmic tails, including many such as talin and kindlins that contain FERM or protein tyrosine-phosphate binding domains; and other proteins that bind to the α tail (Wegener and Campbell, 2008).

EXPERIMENTAL PROCEDURES

Crystallography

α_{IIb} and β_3 ectodomains were fused to C-terminal segments containing a protease site, coiled coils, and tags, with or without α_{IIb}-L959C and β_3-P688C mutations to introduce a disulfide bond, and expressed in CHO Lec 3.2.8.1 cells. Purified α_{IIb}-L959C/β_3-P688C with the C-terminal tag removed by protease in buffer containing 1mM $CaCl_2$ was crystallized in 10% PEG 3350, 50 mM magnesium acetate, and 0.1 M imidazole (pH 7.0). Diffraction data collected at 19-ID of APS was solved using molecular replacement in space group $P4_1$. Final refinement with REFMAC5 utilized TLS and NCS. Crystals contain two molecules per asymmetric unit. Density is present for all ectodomain residues (α_{IIb} 1–959 and β_3 1–690) except for five loops, and, in one molecule, the C-terminal portion of the β tail domain. Thirteen or eighteen N-linked carbohydrate residues are visualized in each molecule. I-EGF1 from the complete $\alpha_{IIb}\beta_3$ ectodomain was used to model density for this domain in rerefined $\alpha_{IIb}\beta_3$ headpiece structures with (Springer et al., 2008) or without Fab (Table 1).

Negative-Stain EM

The clasped and unclasped $\alpha_{IIb}\beta_3$ was purified on a Superdex 200 HR column in Tris saline, 1 mM Ca^{2+}, 1 mM Mg^{2+}. The peak fraction was adsorbed to glow discharged carbon-coated copper grids, stained with uranyl formate, and inspected with an FEI Tecnai 12 electron microscope operated at 120 kV. Images were acquired at a nominal magnification of 67,000 ×. Imaging plates were scanned and digitized with a Ditabis micron imaging plate scanner (DITABIS Digital Biomedical Imaging System, AG, Pforzheim, Germany) using a step size of 15 μm, and 2 × 2 pixels were averaged to yield a final pixel size of 4.46 Å at the specimen level. Between 2000 and 5000 particles were interactively collected, windowed into 75 × 75 pixel individual images, and subjected to ten cycles of multireference alignment and classification. Images were processed and crosscorrelated using SPIDER (Frank et al., 1996) as described (Nishida et al., 2006).

Steered Molecular Dynamics

To build an extended model with closed headpiece, bent $\alpha_{IIb}\beta_3$ was extended at the junction between thigh and calf-1 domains in α and between I-EGF1 and I-EGF2 in β. For extended $\alpha_{IIb}\beta_3$ with open headpiece, we substituted the

headpiece bound to the 10-residue peptide from the C terminus of fibrinogen γ subunit. The same peptide ligand was added to extended-closed $\alpha_{IIb}\beta_3$. Smaller adjustments were made at the hybrid/I-EGF1, I-EGF2/3, and β ankle/β tail interfaces, guided by angles found in other structures and the gimbal-like nature of I-EGF domain interfaces, to retain the calf-2/β tail interface. To accelerate simulations with lateral force, the α and β legs were preseparated by changing the angles between thigh and calf-1 domains and between I-EGF1 and I-EGF2 domains.

During simulations, the N terminus of the ligand (chain C, residue 402) was kept fixed, and forces were applied to the C termini of the integrin $\alpha_{IIb}\beta_3$ ectodomain (α_{IIb}, residue 963 and β_3, residue 690). Models were aligned in the same coordinate system using the β propeller and β I domains. The coordinate system was chosen such that the C termini are confined to the xy plane mimicking the cell membrane, and the centers of masses of β propeller and β I domains are aligned parallel to the y axis. To mimic talin binding, a lateral force of 15 pN was applied at the C terminus of β in the −y direction, away from α, as would occur on cells because of frictional resistance to pulling by α. To mimic tensile force extending the ligand-integrin complex, models were pulled along the −z direction at the C termini of the α_{IIb} and β_3 subunits, each with a force of 15 pN. The xy plane in which the C termini were tethered thus moved in the −z direction. The protein structures were solvated in a 4 Å thick water shell and neutralized with Na ions. Molecular dynamics simulations were with NAMD (Phillips et al., 2005) using the CHARMM22 force fields. The Supplemental Data contains further details and rationale.

Figures

All figures were made with PYMOL.

REFERENCES

Adair, B.D., and Yeager, M. (2002). Three-dimensional model of the human platelet integrin αIIbß3 based on electron cryomicroscopy and x-ray crystallography. Proc. Natl. Acad. Sci. USA 99, 14059–14064.

Alon, R., and Dustin, M.L. (2007). Force as a facilitator of integrin conformational changes during leukocyte arrest on blood vessels and antigen-presenting cells. Immunity 26, 17–27.

Arnaout, M.A., Mahalingam, B., and Xiong, J.P. (2005). Integrin structure, allostery, and bidirectional signaling. Annu. Rev. Cell Dev. Biol. 21, 381–410.

Astrof, N.S., Salas, A., Shimaoka, M., Chen, J.F., and Springer, T.A. (2006). Importance of force linkage in mechanochemistry of adhesion receptors. Biochemistry 45, 15020–15028.

Beglova, N., Blacklow, S.C., Takagi, J., and Springer, T.A. (2002). Cysteine-rich module structure reveals a fulcrum for integrin rearrangement upon activation. Nat. Struct. Biol. 9, 282–287.

Broussard, J.A., Webb, D.J., and Kaverina, I. (2008). Asymmetric focal adhesion disassembly in motile cells. Curr. Opin. Cell Biol. 20, 85–90.

Carrell, N.A., Fitzgerald, L.A., Steiner, B., Erickson, H.P., and Phillips, D.R. (1985). Structure of human platelet membrane glycoproteins IIb and IIIa as determined by electron microscopy. J. Biol. Chem. 260, 1743–1749.

Chen, J., Salas, A., and Springer, T.A. (2003). Bistable regulation of integrin adhesiveness by a bipolar metal ion cluster. Nat. Struct. Biol. 10, 995–1001.

Choi, C.K., Vicente-Manzanares, M., Zareno, J., Whitmore, L.A., Mogilner, A., and Horwitz, A.R. (2008). Actin and alpha-actinin orchestrate the assembly and maturation of nascent adhesions in a myosin II motor-independent manner. Nat. Cell Biol. 10, 1039–1050.

Davis, I.W., Leaver-Fay, A., Chen, V.B., Block, J.N., Kapral, G.J., Wang, X., Murray, L.W., Arendall, W.B., III, Snoeyink, J., Richardson, J.S., et al. (2007). MolProbity: All-atom contacts and structure validation for proteins and nucleic acids. Nucleic Acids Res. 35, W375–W383.

Evans, E.A., and Calderwood, D.A. (2007). Forces and bond dynamics in cell adhesion. Science 316, 1148–1153.

Frank, J., Radermacher, M., Penczek, P., Zhu, J., Li, Y., Ladjadj, M., and Leith, A. (1996). SPIDER and WEB: Processing and visualization of images in 3D electron microscopy and related fields. J. Struct. Biol. 116, 190–199.

Giannone, G., Jiang, G., Sutton, D.H., Critchley, D.R., and Sheetz, M.P. (2003). Talin1 is critical for force-dependent reinforcement of initial integrin-cytoskeleton bonds but not tyrosine kinase activation. J. Cell Biol. 163, 409–419.

Honda, S., Tomiyama, Y., Pelletier, A.J., Annis, D., Honda, Y., Orchekowski, R., Ruggeri, Z., and Kunicki, T.J. (1995). Topography of ligand-induced binding sites, including a novel cation-sensitive epitope (AP5) at the amino terminus, of the human integrin β3 subunit. J. Biol. Chem. 270, 11947–11954.

Hu, K., Ji, L., Applegate, K.T., Danuser, G., and Waterman-Storer, C.M. (2007). Differential transmission of actin motion within focal adhesions. Science 315, 111–115.

Iwasaki, K., Mitsuoka, K., Fujiyoshi, Y., Fujisawa, Y., Kikuchi, M., Sekiguchi, K., and Yamada, T. (2005). Electron tomography reveals diverse conformations of integrin αIIbβ3 in the active state. J. Struct. Biol. 150, 259–267.

Janin, J. (1997). Specific versus non-specific contacts in protein crystals. Nat. Struct. Biol. 4, 973–974.

Kaizuka, Y., Douglass, A.D., Varma, R., Dustin, M.L., and Vale, R.D. (2007). Mechanisms for segregating T cell receptor and adhesion molecules during immunological synapse formation in Jurkat T cells. Proc. Natl. Acad. Sci. USA 104, 20296–20301.

Kim, M., Carman, C.V., Yang, W., Salas, A., and Springer, T.A. (2004). The primacy of affinity over clustering in regulation of adhesiveness of the integrin αLβ2. J. Cell Biol. 167, 1241–1253.

Krissinel, E., and Henrick, K. (2004). Secondary-structure matching (SSM), a new tool for fast protein structure alignment in three dimensions. Acta Crystallogr. D Biol. Crystallogr. 60, 2256–2268.

Lu, C., Takagi, J., and Springer, T.A. (2001). Association of the membrane-proximal regions of the α and β subunit cytoplasmic domains constrains an integrin in the inactive state. J. Biol. Chem. 276, 14642–14648.

Lub, M., van Vliet, S.J., Oomen, S.P., Pieters, R.A., Robinson, M., Figdor, C.G., and van Kooyk, Y. (1997). Cytoplasmic tails of β1, β2, and β7 integrins differentially regulate LFA-1 function in K562 cells. Mol. Biol. Cell 8, 719–728.

Luo, B.H., Springer, T.A., and Takagi, J. (2004). A specific interface between integrin transmembrane helices and affinity for ligand. PLoS Biol. 2, e153.

Luo, B.H., Carman, C.V., and Springer, T.A. (2007). Structural basis of integrin regulation and signaling. Annu. Rev. Immunol. 25, 619–647.

Marlin, S.D., and Springer, T.A. (1987). Purified intercellular adhesion molecule-1 (ICAM-1) is a ligand for lymphocyte function-associated antigen 1 (LFA-1). Cell 51, 813–819.

Miyamoto, S., Akiyama, S.K., and Yamada, K.M. (1995). Synergistic roles for receptor occupancy and aggregation in integrin transmembrane function. Science 267, 883–885.

Moser, M., Nieswandt, B., Ussar, S., Pozgajova, M., and Fassler, R. (2008). Kindlin-3 is essential for integrin activation and platelet aggregation. Nat. Med. 14, 325–330.

Mould, A.P., Barton, S.J., Askari, J.A., Craig, S.E., and Humphries, M.J. (2003). Role of ADMIDAS cation-binding site in ligand recognition by integrin α5β1. J. Biol. Chem. 278, 51622–51629.

Nishida, N., Xie, C., Shimaoka, M., Cheng, Y., Walz, T., and Springer, T.A. (2006). Activation of leukocyte β2 integrins by conversion from bent to extended conformations. Immunity 25, 583–594.

Phillips, J.C., Braun, R., Wang, W., Gumbart, J., Tajkhorshid, E., Villa, E., Chipot, C., Skeel, R.D., Kale, L., and Schulten, K. (2005). Scalable molecular dynamics with NAMD. J. Comput. Chem. 26, 1781–1802.

Puklin-Faucher, E., Gao, M., Schulten, K., and Vogel, V. (2006). How the headpiece hinge angle is opened: New insights into the dynamics of integrin activation. J. Cell Biol. 175, 349–360.

Rocco, M., Rosano, C., Weisel, J.W., Horita, D.A., and Hantgan, R.R. (2008). Integrin conformational regulation: Uncoupling extension/tail separation from changes in the head region by a multiresolution approach. Structure 16, 954–964.

Sheetz, M.P. (1993). Glycoprotein motility and dynamic domains in fluid plasma membranes. Annu. Rev. Biophys. Biomol. Struct. 22, 417–431.

Shi, M., Foo, S.Y., Tan, S.M., Mitchell, E.P., Law, S.K., and Lescar, J. (2007). A structural hypothesis for the transition between bent and extended conformations of the leukocyte β2 integrins. J. Biol. Chem. 282, 30198–30206.

Smith, A., Stanley, P., Jones, K., Svensson, L., McDowall, A., and Hogg, N. (2007). The role of the integrin LFA-1 in T-lymphocyte migration. Immunol. Rev. 218, 135–146.

Springer, T.A., Zhu, J., and Xiao, T. (2008). Structural basis for distinctive recognition of fibrinogen by the platelet integrin αIIbβ3. J. Cell Biol. 182, 791–800.

Takagi, J., Petre, B.M., Walz, T., and Springer, T.A. (2002). Global conformational rearrangements in integrin extracellular domains in outside-in and inside-out signaling. Cell 110, 599–611.

Verschueren, H. (1985). Interference reflection microscopy in cell biology: Methodology and applications. J. Cell Sci. 75, 279–301.

Wegener, K.L., and Campbell, I.D. (2008). Transmembrane and cytoplasmic domains in integrin activation and protein-protein interactions. Mol. Membr. Biol. 25, 376–387.

Xiao, T., Takagi, J., Wang, J.H., Coller, B.S., and Springer, T.A. (2004). Structural basis for allostery in integrins and binding of fibrinogen-mimetic therapeutics. Nature 432, 59–67.

Xiong, J.P., Stehle, T., Diefenbach, B., Zhang, R., Dunker, R., Scott, D.L., Joachimiak, A., Goodman, S.L., and Arnaout, M.A. (2001). Crystal structure of the extracellular segment of integrin αVβ3. Science 294, 339–345.

Xiong, J.P., Stehle, T., Zhang, R., Joachimiak, A., Frech, M., Goodman, S.L., and Arnaout, M.A. (2002). Crystal structure of the extracellular segment of integrin αVβ3 in complex with an Arg-Gly-Asp ligand. Science 296, 151–155.

Xiong, J.P., Stehle, T., Goodman, S.L., and Arnaout, M.A. (2004). A novel adaptation of the integrin PSI domain revealed from its crystal structure. J. Biol. Chem. 279, 40252–40254.

Yan, B., and Smith, J.W. (2001). Mechanism of integrin activation by disulfide bond reduction. Biochemistry 40, 8861–8867.

Ye, F., Liu, J., Winkler, H., and Taylor, K.A. (2008). Integrin alpha IIb beta 3 in a membrane environment remains the same height after Mn2+ activation when observed by cryoelectron tomography. J. Mol. Biol. 378, 976–986.

Zhu, J., Boylan, B., Luo, B.H., Newman, P.J., and Springer, T.A. (2007a). Tests of the extension and deadbolt models of integrin activation. J. Biol. Chem. 282, 11914–11920.

Zhu, J., Carman, C.V., Kim, M., Shimaoka, M., Springer, T.A., and Luo, B.H. (2007b). Requirement of α and β subunit transmembrane helix separation for integrin outside-in signaling. Blood 110, 2475–2483.